Dalton Transactions

Accepted Manuscript

ROYAL SOCIETY OF CHEMISTRY

www.rsc.org/dalton

Dalton Transactions

RSCPublishing

ARTICLE

Active layer solution-processed NIR-OLEDs based on ternary erbium(III) complexes with 1,1,1-trifluoro-2,4-pentanedione and different N,N-donors

Cite this: DOI: 10.1039/x0xx00000x

Received 00th January 2012,
Accepted 00th January 2012

DOI: 10.1039/x0xx00000x

www.rsc.org/

P. Martín-Ramos[a], C. Coya-Párraga[b], V. Lavín[c], I. R. Martín[c], M. Ramos Silva[d], P.S. Pereira Silva[d], M. García-Vélez[b], A.L. Álvarez[b] and J. Martín-Gil[a*]

Using a fluorinated 1,1,1-trifluoro-2,4-pentanedione (Htfac) ligand and either 2,2'-bipyridine (bipy), bathophenanthroline (bath) or 5-nitro-1,10-phenanthroline ($5NO_2$phen) as ancillary ligands, three new ternary erbium(III) octacoordinated complexes have been synthetized. The single crystal structures of the new complexes (namely [Er(tfac)$_3$(bipy)], [Er(tfac)$_3$(bath)] and [Er(tfac)$_3$($5NO_2$phen)]) have been determined and their properties investigated by Fourier Transform infrared (FTIR) spectroscopy, Raman spectroscopy and thermodynamic analysis. After ligand-mediated excitation of these complexes in the UV, they all show the characteristic near infrared (NIR) luminescence of the corresponding Er^{3+} ion at 1532 nm. This same emission in the C-band transmission window can also be obtained from the solution-processed organic light-emitting diodes (OLEDs) with structure glass/ITO/PEDOT:PSS/[Er(tfac)$_3$(N,N-donor)]/Ca/Al. In spite of the fact that the photoluminescence intensity of [Er(tfac)$_3$($5NO_2$phen)] is stronger than those of [Er(tfac)$_3$(bipy)] and [Er(tfac)$_3$(bath)], the best electroluminescence results correspond to the OLED based on [Er(tfac)$_3$(bath)] complex, as a consequence of the superior electron transport capabilities of bathophenanthroline.

Introduction

The study of rare earth element complexes with luminescence properties began in 1942 when Weissman reported that lanthanide β-diketonate complexes exhibit luminescence when irradiated with ultraviolet light.[1] Since then, the 1.53 μm emission (either photoluminescent or electroluminescent) from Er^{3+} complexes has been deemed as particularly attractive for optoelectronic devices. Therefore, the development of materials which allow operation at 1.53 μm, for example the electroluminescent (EL) emission from Er^{3+} complexes-based OLEDs, has become an interesting subject.[2] Unfortunately, this NIR emission is usually weak due to the fact that conventional β–diketone ligands contain O-H and C-H oscillators which – when coordinated to the lanthanide ion– increase the non-radiative decay rates of the rare earth excited states, particularly for the lowest energetic transitions. According to the literature, the replacement of C-H bonds with lower-energy C-F oscillators is able to lower the vibration energy of the ligand, which in turn decreases the energy loss caused by ligand vibration and enhances the emission intensity of the Er^{3+} ion.[3]

On the other hand, OLED technology has reached a level of maturity in which the reduction of manufacturing costs and the adaptation of procedures to mass-production techniques play a key role. In this context, wet coating processes are in the spotlight due to their compatibility with inexpensive manufacturing techniques for large area operation, such as ink-jet printing or roll-to-roll systems. Consequently, amenability to solution processing has become a fundamental prerequisite for large area, low-cost mass production, and is to be paid particular attention when designing materials for organic active layers. Recently, we have demonstrated two other full-solution processed NIR-emitting OLEDs[4,5] but an analysis on the impact of the diimide ancillary ligand choice on the EL properties for 'complex-only' emission layer-based devices (i.e., without resourcing to a host:guest system) has –to the best of our knowledge– not been reported so far. For an analysis of the impact of the β-diketone moiety choice on PL and EL, the reader is referred, for example, to references [6] and [7], respectively.

In this work, we present the structural and photophysical properties of three novel Er^{3+} complexes with general formula [Er(tfac)$_3$(N,N-donor)], in which the fluorinated 1,1,1-trifluoro-2,4-pentanedione (Htfac) β-diketone ligand has been chosen as the main sensitizer and either 2,2'-bipyridine (bipy), bathophenanthroline (bath) or 5-nitro-1,10-phenanthroline

($5NO_2$phen) have been used as ancillary ligands. Steady and time-resolved photoluminescence studies demonstrate how the Er^{3+} emission at 1.53 μm can be efficiently sensitized through direct excitation of the organic ligands by the so-called *antenna effect*, in which energy is transferred from the lowest triplet states of the ligands to the excited states of the central Er^{3+} ion. This ligand-mediated sensitization of Er^{3+} is affected by the neutral N,N-donor choice, and so should be the EL properties for the solution-processed OLEDs. Thus, their impact on the *J–V* and electro-luminescence responses for full-solution processed devices with structure glass/indium-tin oxide (ITO)/poly(3,4-ethylenedioxythiophene)–poly(styrenesulfonate) (PEDOT:PSS) /[Er(tfac)$_3$(N,N-donor)]/Ca/Al is also assessed.

Results and discussion

Structural description

In the three structures (Figure 1, Table 1), three negative *β*-diketonate ligands and one N,N-donor moiety coordinate the Er^{3+} ion. The environment around the rare earth has a slightly distorted square-antiprismatic configuration, with one top square face containing the two N atoms and two O atoms and the bottom square face containing the remaining four O atoms. The angle between the mean planes of such faces ranges between 1º and 4º in the three compounds.

All compounds show some signs of structural disorder: [Er(tfac)$_3$(bipy)] has a random interchange of the bipyridine moiety with one (1,1,1-trifluoro-2,4-pentanedione), simulating an inversion symmetry around the Er^{3+} ion, and its CF_3 groups are also disordered; in [Er(tfac)$_3$(bath)] and [Er(tfac)$_3$($5NO_2$phen)] there is evidence of a mild disorder due to the large terminal ellipsoids, specially of the F atoms.

5-nitro-1,10-phenanthroline and bathophenanthroline complexes show similar Er–N and Er–O distances (Table 2), in good agreement with their average values[8]. On the other hand, the Er–O and the Er–N distances for the complex with 2,2'-bipyridine are on the upper limit and on the lower limit of their respective usual ranges[8], but most probably this apparent nonconforming values are due to the heavy disorder around the Er^{3+} and the difficulty to precisely locate the coordinating atoms.

None of the three compounds show intermolecular interactions other than Van der Waals.

[Er(tfac)$_3$(bipy)] and [Er(tfac)$_3$(bath)] pack very efficiently, leaving no solvent accessible voids. [Er(tfac)$_3$($5NO_2$phen)] shows voids up to 34 Å^3.

Table 1.Crystal data and structure refinement

Complex	[Er(tfac)$_3$(bipy)]	[Er(tfac)$_3$(bath)]	[Er(tfac)$_3$($5NO_2$phen)]
Empirical formula	$C_{25}H_{20}ErF_9N_2O_6$	$C_{39}H_{28}ErF_9N_2O_6$	$C_{27}H_{19}ErF_9N_3O_8$
Formula weight	782.69	958.89	851.71
Temperature (K)	293(2)	293(2)	293(2)
Wavelength (Å)	0.71073 Å	0.71073 Å	0.71073 Å
Crystal system	Monoclinic	Monoclinic	Monoclinic
Space group	*C*2/*c*	$P2_1/c$	$P2_1/c$
a (Å)	22.705(5)	17.2382(4)	9.7956(9)
b (Å)	9.2115(18)	16.2042(3)	14.8137(15)
c (Å)	15.646(3)	14.0954(3)	24.0161(18)
β (º)	118.042(3)	102.4740(10)	114.072(3)
Volume (Å^3)	2888.2(10)	3844.34(14)	3181.9(5)
Z	4	4	4
Density (calculated, g cm^{-3})	1.800	1.657	1.778
Absorption coefficient (mm^{-1})	3.005	2.275	2.741
F(000)	1524	1892	1660
Crystal size (mm^3)	0.22×0.11×0.04	0.20×0.10×0.03	0.13×0.07×0.06
θ range for data collection (º)	2.03-25.69	1.74-25.73	1.66-26.16
Index ranges	-27<*h*<25; -11<*k*<10; -8<*l*<19	-21<*h*<21; 19-<*k*<19; -17<*l*<17	-12<*h*<12; -18<*k*<18; -29<*l*<29
Reflections collected	6054	72839	64512
Independent reflections	1826	4969	3246
Completeness to 2*θ*=51º	0.988	0.999	0.983
Refinement method	Full matrix LS on F^2	Full matrix LS on F^2	Full matrix LS on F^2
Data/restrains/parameters	2714/37/220	7322/0/517	6250/0/436
Goodness-of-fit on F^2	1.049	1.006	1.037
Final *R* indices [*I*>2σ(*I*)]	*R*=0.0725; w*R*=0.1977	*R*=0.0377; w*R*=0.0784	*R*=0.0670; w*R*=0.1639
R indices (all data)	*R*=0.1059; w*R*=0.2395	*R*=0.0763; w*R*=0.0929	*R*=0.1459; w*R*=0.1960
Largest diff. peak and hole	1.426/-2.643	0.789/-0.555	0.687/-1.837

Table 2. Selected distances (Å)

Bond	[Er(tfac)$_3$(bipy)]	[Er(tfac)$_3$(bath)]	[Er(tfac)$_3$($5NO_2$phen)]
Average Er–N	2.365	2.518	2.550
Average Er–O	2.362	2.310	2.301

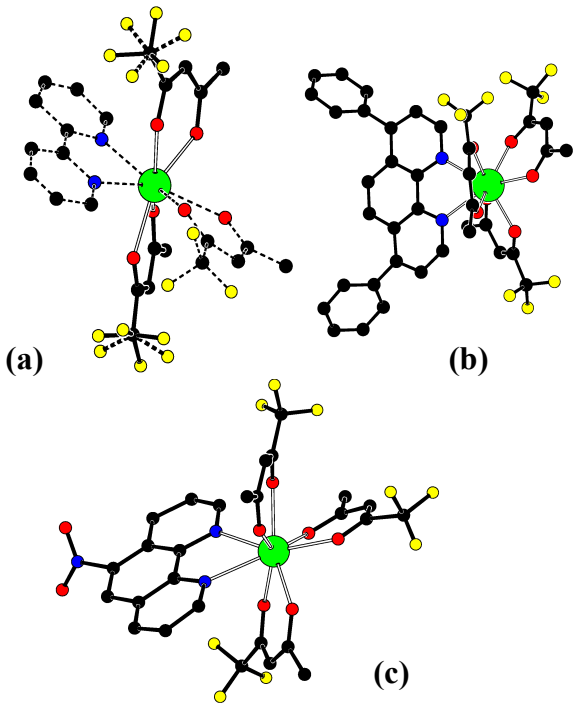

Figure 1. Structural diagrams of *(a)* [Er(tfac)$_3$(bipy)], *(b)* [Er(tfac)$_3$(bath)] and *(c)* [Er(tfac)$_3$(5NO$_2$phen)]. In *(a)*, H atoms were omitted for clarity. In (a), for clarity, only one of the alternative conformations is shown.

X-ray powder diffraction

The experimental diffraction patterns for the three Er^{3+} complexes are shown in Figure 2, together with simulated powder patterns obtained from the single crystal structure using PLATON[9]. There is an excellent match between simulated and experimental diffractograms: the peaks appear at the predicted theta angles at the same relative intensities. The experimental diffractograms show a background higher for low theta angles as expected from the diffuse scattering of X-rays by glass and air, a common characteristic when using rotating capillaries in a Debye-Scherrer geometry. Powder diffraction shows that all the material synthesized contains the same structure as the small single crystals used for single-crystal X-ray diffraction.

Differential Scanning Calorimetry

Regardless of the differences which can be observed in the DSC curves (Figure 3) of the studied complexes, ([Er(tfac)$_3$(bipy)] shows endothermic effects at 186ºC, 224ºC, exothermic effects at 305ºC and 321ºC and a main thermal exothermic effect at 342ºC; [Er(tfac)$_3$(bath)] only shows two endotherms at 245ºC and 337ºC; and [Er(tfac)$_3$(5NO$_2$phen)] only two main exotherms at 246ºC and 310ºC), it can be established that the complexes exhibit relatively high thermal stability. The highest stability is attained for the bipy complex, whose thermal effects are shifted to higher temperatures in comparison to the other two.[10]

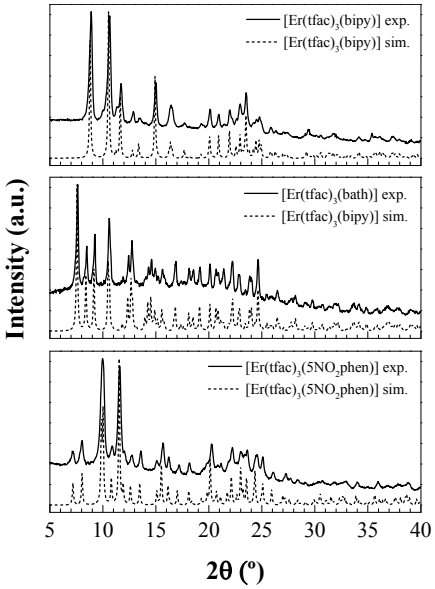

Figure 2. Comparison between experimental and simulated diffraction patterns

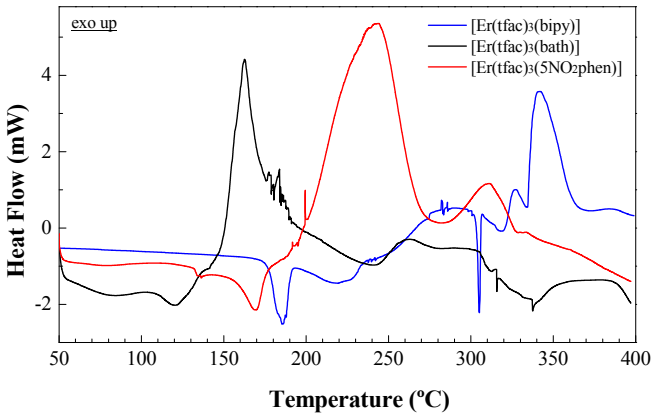

Figure 3. DSC curves for the three novel complexes.

Infrared spectroscopy

FTIR spectra of the reported complexes (Figure 4) show a weak absorption in the 3500-3000 cm^{-1} region, attributed to OH stretching vibrations, which is the expected for a low amount of OH groups, as planned in the preparative conditions.

The absorption bands with variable intensity which appear in the frequency range 1624-1431 cm^{-1} correspond to aromatic ring vibrations of N,N-donor molecules and the tfac anions and C=O groups of anions.[11]

In the region between 1400 and 900 cm^{-1} bands characteristic of the C=N ring vibrations of N,N-donors appear at around 1470 cm^{-1} and those assigned to the in-plane bending of C–H bonds at 1225–1188 cm^{-1}.

An important feature – provided that these are fluorinated complexes – is the occurrence of strong carbon–fluorine bands around 1140 cm^{-1}, particularly the one which appears between 1162 and 1137 cm^{-1}, assigned to CF_3 as (C–F) stretching modes.[12]

In the frequency range 900-575 cm^{-1} the spectra exhibit the absorption bands characteristic of coordinated N,N-donor molecules: 646, 740 and 764 cm^{-1} for the complex containing 2,2'-bipyridine; 637, 735, 755 and 788 cm^{-1} for the complex containing bathophenanthroline ancillary ligand, and 737, 749 and 836 cm^{-1} for the complex with 5-nitro-1,10-phenanthroline. Among these bands, the CH twisting bending vibrations at around 840 and 750 cm^{-1} are appreciably red shifted (*vs*. those of free ligands) due to the perturbation induced by their coordination to the metal ion.

Finally, the band at around 432 cm^{-1}, which corresponds to ν(Er–O) vibration, and the peak at 561 cm^{-1}, which should assigned to a ν(Er–N) vibration, also offer evidence of the fact that coordination bonds have been formed between erbium and Htfac, and erbium and diimide, respectively.[13]

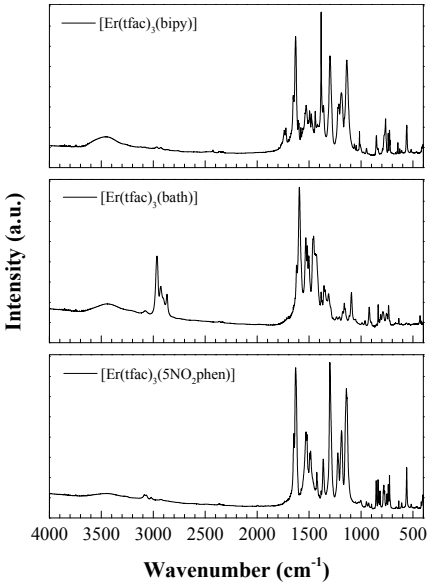

Figure 4. Infrared spectra of the novel complexes

Raman spectra

Raman spectra of the complexes (Figure 5) show a strong multiple peak between 1626 and 1571 cm^{-1}, attributed to the C=N and C=O bonds from coordinated N,N-donor molecules and *β*-diketonate, respectively.

Peaks at around 1455 cm^{-1} [ν (C=C, C=N)], 1355 cm^{-1} [ν(C=C) + δ (CH)], 1050 cm^{-1} (ring breathing) and 725 cm^{-1} [δ(CH)] are also characteristic of coordinated N,N-donors.

Since they are fluorinated compounds, ν(C–F) modes appear at 1065-1052 cm^{-1}.

In relation to the bands in the 100–500 cm^{-1} region, they can either be ascribed to the neutral ligands (provided that the bands of the bipy and phen-derivative ligands are only marginally affected by the complexation, displaying small wavenumber shifts or intensity changes)[14] or to the symmetrical and asymmetrical Er–O and Er–N stretching modes (*viz*., 290, 333-338, 390–392 and 421 cm^{-1}).

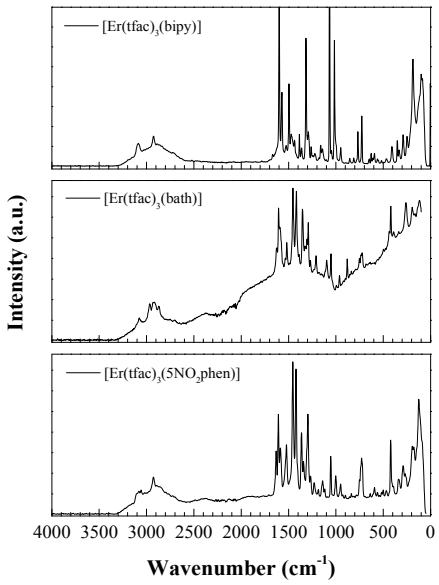

Figure 5. Raman spectra of the novel complexes

NRM spectroscopy

^{1}H-NMR. The ^{1}H-NMR spectra of the [Er(tfac)$_3$(N,N-donor)] complexes display, apart from two strong signals at 3.3 and 4.9 ppm corresponding to CD_3OD, two signals associated to the tfac *β*-diketonate: at 2.1 ppm for methyl protons and at 3.6 ppm for methine protons (see the spectrum of [Er(tfac)$_3$(5NO$_2$phen)] complex in Figure 6). The other signals which appear in the 8.2-9.4 ppm range can be assigned to protons of the diimide ligands, in close agreement with those expected from Mnova 9.0.1 (Mestrelab Research SL) calculations.

^{19}F-NMR. The ^{19}F-NMR spectra of the complexes (e.g., see inset in Figure 6) display only one strong signal at ca. -80.1 ppm due to $–CF_3$ groups.

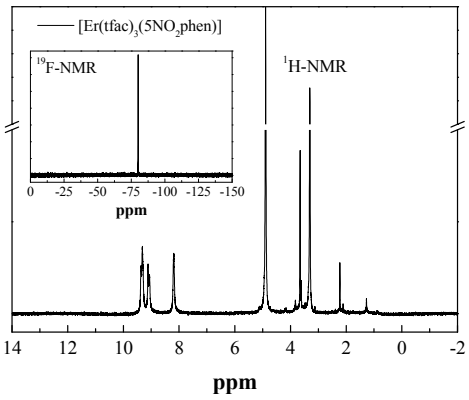

Figure 6. ^{1}H-NMR and ^{19}F-NMR (*inset*) spectra for [Er(tfac)$_3$(5NO$_2$phen)] complex.

Absorption and emission spectra

Figure 7a shows the absorption spectra for the Er^{3+} complexes in 10^{-5} M methanol diluted solutions. The main absorption

bands are associated to the tfac *β*-diketonate ligand π-π* transitions with maxima in the 290-295 nm range.[15] Other sharp *f-f* transitions from the $^4I_{15/2}$ ground state of the Er^{3+} ion may also be observed, overlapped with the organic ligands absorption. Increasing the concentration to 10^{-3} M allow us to better resolve these Er^{3+} transitions: Figure 7b shows that the strongest transitions correspond to $^4G_{11/2}$ (378 nm) – in [Er(tfac)$_3$(bipy)] – and to the structured $^2H_{11/2}$ (519 nm) plus $^4S_{3/2}$ (543 nm) absorptions. It is also possible to observe the transitions associated to $^4F_{5/2}$,$^4F_{3/2}$ (451 nm), $^4F_{7/2}$ (488 nm) and $^4F_{9/2}$ (655 nm) levels of the Er^{3+} ion.[16]

The most intense *f-f* absorption band corresponds to $^4I_{15/2}\rightarrow{}^2H_{11/2}$ hypersensitive transition, whose intensity depends on the site symmetry and anisotropy.[17] Although the three complexes are eight-coordinated, the solvent (methanol) effect on the hypersensitive transitions is dissimilar. It is interesting to associate these results with the basicity of the heterocyclic ligands (bipy, bath and 5NO$_2$phen). Bathophenanthroline is more basic (pKa=4.67) than 2,2'-bipyridine (pKa=4.38), while 5-nitro-1,10-phenanthroline has the lowest basicity (pKa=3.33). Being the most basic, bath would be expected to contribute more electron density through Er–N bond making the Er^{3+} ion more electron rich. As a result, the Er^{3+} will show less attraction for electron donor solvents. The rigidly planar structure of bath would also be helpful in obstructing the coordination of solvent molecules to inner coordination sphere of Er^{3+} and restricting the complex–solvent interaction[18] (in fact, there are no solvent accessible voids, as discussed above).

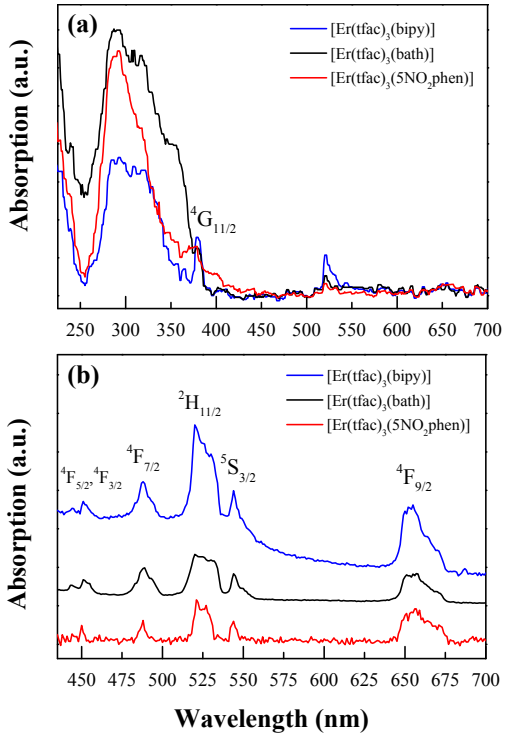

Figure 7. Optical absorption spectra in (*a*) 10^{-5} M methanol diluted solutions and (*b*) 10^{-3} M methanol diluted solutions.

Photoluminescent emission in solid state

The emission of the novel Er^{3+} complexes in the visible region has been studied under direct excitation of the organic ligands at λ=405 nm‡ (Figure 8a). Under this direct excitation, ground state absorption $S_0\rightarrow S_1$ in the ligand moiety occurs, followed by fast vibrational relaxation to the lowest vibrational level of the excited singlet level, from which it can relax by radiative emission of a photon at around 420 nm or it may undergo intersystem crossing (ISC) to the triplet level due to spin reorientation, from which subsequent resonant energy transfer (ET) to Er^{3+} may take place. Since the emission spectra have been measured in powder, it is expected that they may be slightly red-shifted in comparison to those obtained in solution, as a result of the aggregation state.

It should be pointed out that the emission intensity of the organic ligand for the [Er(tfac)$_3$(5NO$_2$phen)] complex is significantly weaker than those of the other two complexes (39% of that from [Er(tfac)$_3$(bath)] and 58% of that from [Er(tfac)$_3$(bipy)] at the peak). It is worth noting that, even though the intensities of the spectra in powder form cannot be strictly compared, a qualitative estimation is reasonable provided that we can assume the same incident energy density. This quenching of the visible emission of the complexes is related to the efficiency of the energy transfer capability from the ligand to the fundamental transition of the Er^{3+} ion, the so-called *antenna effect*. At the same time, the intensity of the characteristic $^4I_{13/2}\rightarrow{}^4I_{15/2}$ NIR emission of the Er^{3+} transition is expected to be favoured.

Figure 8b shows a qualitative comparison between the Er^{3+}: $^4I_{13/2}\rightarrow{}^4I_{15/2}$ transition emission intensities at room temperature for the three complexes excited with a laser radiation at 532 nm, resonant with the $^4I_{15/2}\rightarrow{}^2H_{11/2}$ transition, provided that all the samples were measured in the same conditions, as mentioned above. The band structure is very similar for the three complexes, with maximum at 1532 nm, and additional weaker bands surrounding. This structure is mainly due to the Stark energy levels hyperfine structure and the electron population distributions of the $^4I_{13/2}$ and $^4I_{15/2}$ multiplets. It is noticeable that [Er(tfac)$_3$(5NO$_2$phen)] complex PL emission is the most intense.

In order to evaluate the energy transfer by *antenna effect,* the measurements have also been conducted under direct excitation of the organic ligand at λ=337 nm, with analogous results. In this case, the band structures for [Er(tfac)$_3$(bipy)] and [Er(tfac)$_3$(bath)] are quite similar to those obtained by direct excitation of Er^{3+} (inset in Figure 8b), showing a maximum at 1532 nm and some structure related with the Stark energy level and electron population distributions of $^4I_{13/2}$ and $^4I_{15/2}$ multiplets. Conversely, for [Er(tfac)$_3$(5NO$_2$phen)], its emission upon ligand excitation is accompanied by a strong reabsorption associated to $^4I_{13/2}$ level (ca. 1500 nm), probably due to a concentration effect. When the measurements were repeated in deuterated methanol solutions (Figure S1†), this effect was not present anymore, and the three spectra showed similar band structures.

The fact that the NIR emission intensity of the [Er(tfac)$_3$(5NO$_2$phen)] complex under ligand excitation was higher than those of the other two complexes under the same experimental conditions, together with the quenching of the organic ligand emission (mentioned above), is indicative of an improved energy transfer from the organic ligand to the Er^{3+} ion in the resulting environment of [Er(tfac)$_3$(5NO$_2$phen)] complex, in agreement with previous findings.[4,5]

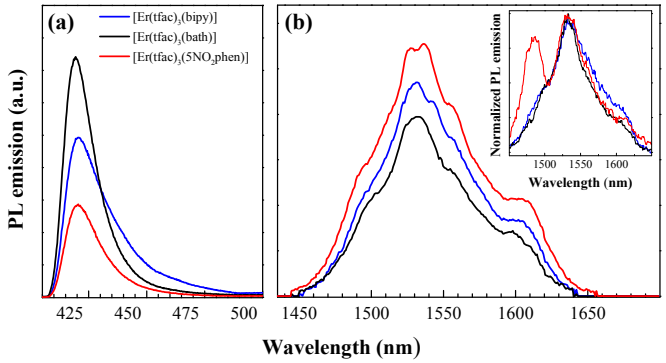

Figure 8. PL emission in (*a*) the visible region and (*b*) in the near-infrared region (upon $^2H_{11/2}$ level direct excitation). The inset in (*b*) shows a comparison of the normalized spectra upon excitation of the organic ligand in the UV region.

Excitation spectra: The excitation spectra of the complexes monitored at 1540 nm (see Figure 9) feature a common band at ca. 380 nm that can be ascribed to the tfac *β*-diketonate and other bands at lower wavelengths associated to the different heterocyclic ligands: 2,2'-bipyridine has a single band at 350 nm, bathophenanthroline shows three bands at 325, 343 and 361 nm, and 5-nitro-1,10-phenanthroline displays two bands at 320 and 359 nm.[19] These bands can be attributed to their respective ligand-centered ($S_0 \rightarrow S_n$) transitions, and the shift between UV-Vis absorption and excitation peaks is consistent with the literature (e.g., [20]). Thus, aforementioned *antenna effect* sensitization mechanism is further confirmed.

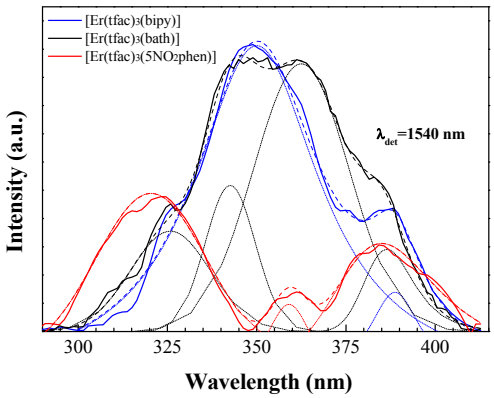

Figure 9. Excitation spectra (*solid lines*) and deconvolutions using modified Gaussian fits (*dotted and dashed lines*) of the three complexes. A qualitative comparison of the intensities is not applicable in this case, provided that the amount of sample for [Er(tfac)$_3$(5NO$_2$phen)] was significantly smaller.

Lifetime measurements: emission dynamics. The dynamics of the PL decay of the organic ligands (Figure 10a) upon excitation with a high-repetition rate pulsed picosecond laser at λ=405 nm confirm the stationary PL results discussed above, since longer ligand lifetimes lead to more intense emission in the visible region. The studied $S_1 \rightarrow S_0$ radiative decay times – determined using FAST® software for the deconvolution of the instrument response function (IRF) and the exponential component analysis– are 0.56 and 1.02 ns for [Er(tfac)$_3$(bipy)] and [Er(tfac)$_3$(bath)], respectively. The decay time for the [Er(tfac)$_3$(5NO$_2$phen)] is much faster, almost comparable to the IRF, and thus could not be accurately deconvoluted. These ligand lifetimes are in good agreement with the intensities of the PL spectra discussed above: as expected, the most efficient antenna effect is shown by [Er(tfac)$_3$(5NO$_2$phen)] complex, which has the shortest ligand decay time value, provided that excited state energy is more efficiently transferred to the Er^{3+} (by ISC and subsequent resonant energy transfer, RET).

The PL decays of the $^4I_{13/2}$ multiplet were measured after $^4I_{11/2}$ excitation (980 nm) and show a single exponential behaviour, which can be observed as a linear dependence in the semi-log representations in Figure 10b. Quite similar decay times have been found for the three complexes, both in powder form and in CD_3OD solutions, with time constants of 1.65, 1.40 and 1.35 μs for [Er(tfac)$_3$(bipy)], [Er(tfac)$_3$(bath)] and [Er(tfac)$_3$(5NO$_2$phen)], respectively. These values, typical of lanthanide complexes (and far smaller than the emission decay time of the isolated ion), are due to vibronic coupling with high energy C–H stretching vibrations in the neighbourhood of the Er^{3+} ion (originated from the remaining non-fluorinated part of the ligands), which lead to quenching of the excited state (because of the relatively small energy gap between the excited state $^4I_{13/2}$ and the ground state). Nonetheless, it must be noted that these complexes show a significant reduction of the non-radiative losses caused by O–H and N–H oscillators, which have the most deleterious effects on the emission, and that the partial fluorination of the *β*-diketonates leads to an increase in the lifetime ranging from 30% to 60% (analogous non-fluorinated complexes show lifetime values around 1 μs).[21] Taking into account that the radiative lifetime (τ_{rad}) of Er^{3+} ranges τ=2–3 ms, the quantum efficiency of these compounds is $\eta=\tau/\tau_{rad}$~0.1%.

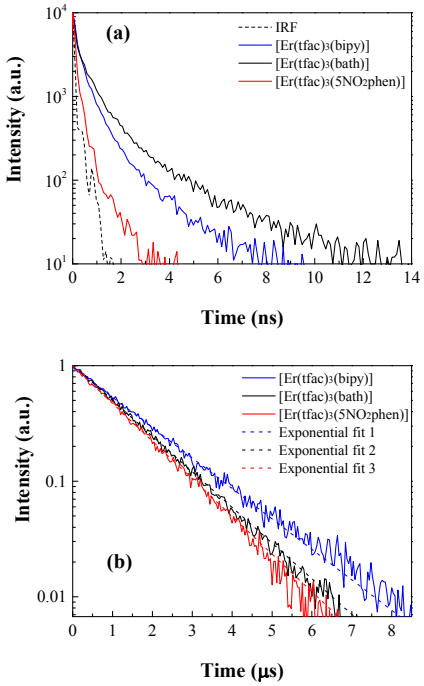

Figure 10. (*a*) PL lifetime values for the ligands-associated emission in the visible region and (*b*) Er^{3+}:$^4I_{13/2}\rightarrow{}^4I_{15/2}$ emission lifetime values for the three complexes.

Device properties: electroluminescent emission and current-voltage characteristics

The good uniformities and suitable thicknesses observed in the control layers on glass substrates have encouraged the application of these complexes as emission layers in solution-processed devices. The OLEDs' structure was glass/ITO/PEDOT:PSS/[Er(tfac)$_3$(N,N-donor)]/Ca/Al, fabricated according to the described experimental method.

Figure 11 shows the current density-voltage (*J*–*V*) responses and the electroluminescent emissions recorded from the OLEDs. With regard to the *J*-*V* characteristics, the [Er(tfac)$_3$(bath)]-based device exhibits the lowest threshold voltage (V_T=4V, Figure 11a) of the three, followed by that based on [Er(tfac)$_3$(bipy)] (V_T=6V, inset in Figure 11c) and, lastly, by the [Er(tfac)$_3$(5NO$_2$phen)]–based device (V_T≈11V, Figure 11c).

In relation to the EL behavior, emission associated to Er^{3+}:$^4I_{13/2}\rightarrow{}^4I_{15/2}$ transition was obtained for the devices with [Er(tfac)$_3$(bath)] (Figure 11b) and [Er(tfac)$_3$(5NO$_2$phen)] (Figure 11d) active layers. Conversely, the [Er(tfac)$_3$(bipy)]-based device did not show electroluminescent emission. This is consistent with the poor charge transport properties of 2,2'-bipyridine: to the best of the authors' knowledge, all examples of OLEDs based on *β*-diketonate complexes with bipy ancillary ligand resort to the use of host:guest systems in which complexes are blended with a polymer matrix (usually poly(9-vinylcarbazole) (PVK)[22]). The few exceptions in which the devices successfully used the pure complexes "as-is" (deposited either by thermal deposition or from solution) involved *β*-diketonates with aromatic substituents which could enhance the charge transport.[4,7]

In the other two devices, the NIR EL emission spectra, peaking at 1.53 μm, matches very well with the PL spectra, except for a narrowing at the low-energy wing of the band. This effect is most likely related to an increase in the temperature of the material and consequently to the redistribution of the electronic population in the excited $^4I_{13/2}$ multiplet. Since no residual ligand-associated EL emission in the visible range could be detected, an efficient charge transfer (i.e., exciton harvest processes) from the organic ligands to the central Er^{3+} ion can be assumed. Thus, the *antenna effect* energy-transfer mechanism discussed for the PL may also occur when the emission is excited *via* an applied voltage.

Figure 11b shows the EL emission spectra of [Er(tfac)$_3$(bath)] measured both at the onset of this emission for a 1.2 mA driving current (16 mA/cm^2 @ 4.5 V) and for 5 mA (71 mA/cm^2 @ 6.2 V); while the EL emission spectra of [Er(tfac)$_3$(5NO$_2$phen)] measured at 2.5 mA driving current (79.57 mA/cm^2 @ 21.1 V) is shown in Figure 11d. Since the EL spectra were recorded in the same conditions, the integrated area divided by the current density can provide a rough estimation of the emission efficiencies in order to compare the two devices. Thus, we obtain 5×10^{-4} and 1.6×10^{-4} counts·mA^{-1}·cm^2 for the [Er(tfac)$_3$(bath)] and the [Er(tfac)$_3$(5NO$_2$phen)]-based devices, respectively. The enhanced performance of the device based on the [Er(tfac)$_3$(bath)] complex -in terms of its lower threshold voltage, lower driving current and higher EL efficiency- may be explained by the superior electron transport capabilities of bathophenanthroline,[23] although several other factors can also affect the EL efficiency. Moreover, the obtained V_T value for the [Er(tfac)$_3$(bath)] based device is lower than that previously reported by Wei *et al.*[24] for a multilayer vacuum-deposited device (7 V, similar to that reported for a solution-processed device in [5]) and further lower than that reported for the ErQ-based device.[25]

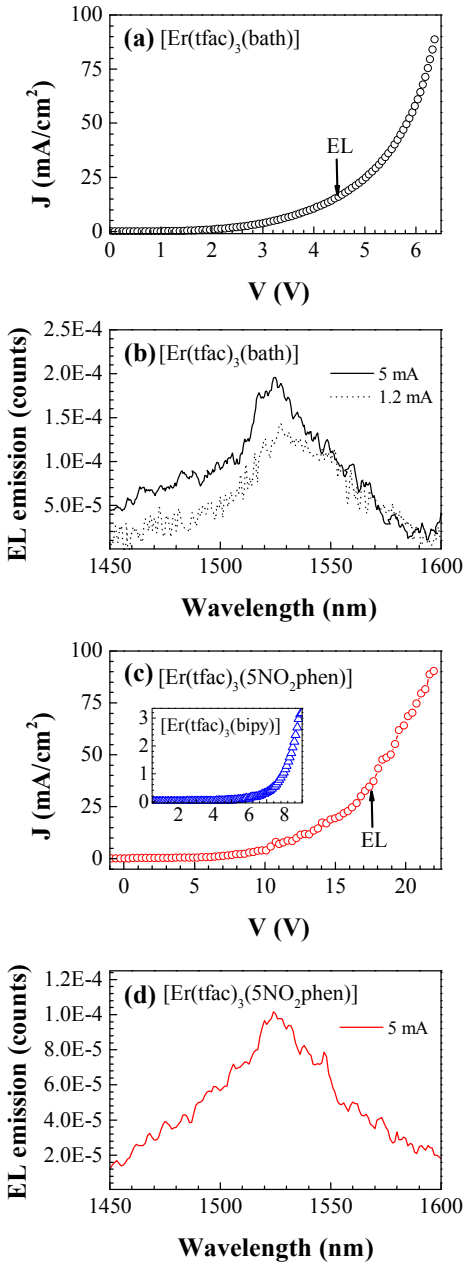

Figure 11. Recorded *J–V* curves and EL emissions of the [Er(tfac)$_3$(bath)] ((*a*) and (*b*)) and [Er(tfac)$_3$(5NO$_2$phen)]-based ((*c*) and (*d*)) devices. The arrows in (*a*) and (*c*) indicate their respective EL onsets, that is, 16 mA/cm^2 @ 4.5 V and 34.5 mA/cm^2 @ 17.4 V. The inset in (*c*) shows the *J-V* curve for the OLED with [Er(tfac)$_3$(bipy)] active layer.

Conclusions

Three novel highly-coordinated Er^{3+} complexes with the same fluorinated *β*-diketonate ligand (tfac) and different neutral diimide ligands (namely 2,2'-bipyridine, bathophenanthroline and 5-nitro-1,10-phenanthroline) have been synthesized and characterized with a view to their application as chromophores and, in particular, as active layers in full solution-processed NIR-OLEDs. Single crystal X-ray structures, powder diffraction, FTIR, Raman and DSC data are reported.

Through a characterization of their photophysical properties, we have been able to confirm a significant energy transfer by an *antenna effect*, i.e., NIR emission at 1.53 µm from the Er^{3+} ions can be efficiently achieved by exciting the organic ligands in the UV region due to ligand to metal ET processes. The 5-nitro-1,10-phenanthroline N,N-donor proves to be particularly well suited for this purpose.

Two of the complexes (those with bath and 5NO$_2$phen) have been successfully incorporated as emission layers into full-solution processed organic light-emitting diodes, with structure glass/ITO/PEDOT:PSS/[Er(tfac)$_3$(N,N-donor)]/Ca/Al, taking advantage of their good thin film and charge transport properties, and without resourcing to host:guest systems. These devices, when excited with an applied voltage, show EL emission in C-band, suitable for third communication window applications in fiber optics. Their comparison shows, that in spite of the fact that the PL intensity of [Er(tfac)$_3$(5NO$_2$phen)] is stronger than that of [Er(tfac)$_3$(bath)], the best electroluminescence results correspond to the OLED based on the [Er(tfac)$_3$(bath)] complex, as a consequence of the superior electron transport capabilities of bathophenanthroline. Considering the lower threshold voltage, lower driving current and higher efficiency parameters of the later device, bath ancillary ligand appears as the most promising choice for further developments.

Experimental

Materials, synthesis and analytical data

All reagents and solvents employed were commercially available and used as supplied without further purification. All the procedures for complex preparation were carried out under nitrogen environment and using dry reagents to avoid the presence of water and oxygen, which can quench Er^{3+} photoluminescence.

Complex [Er(tfac)$_3$(bipy)] was obtained as follows: under stirring, 1,1,1-trifluoro-2,4-pentanedione (3 mmol) methanol solution (20 ml) was added to a 1 mmol of $Er(NO_3)_3{\cdot}5H_2O$ in methanol. The mixture was neutralized by adding potassium methoxide (3 mmol) dropwise under vigorous stirring until potassium nitrate precipitated. KNO_3 was removed by decanting, and 2,2'-bipyridine (1 mmol) was finally added. The mixture was heated to 75 ºC and stirred overnight, then washed with dioxane, and finally dried in vacuum to give product in 90-95% yield (based in Er). Crystals suitable for X-ray analysis were obtained by slow evaporation of a methanol-dioxane solution at room temperature. Synthesis procedure for [Er(tfac)$_3$(bath)] and [Er(tfac)$_3$(5NO$_2$phen)] was analogous, using 1 mmol of bathophenanthroline or 5-nitro-1,10-phenanthroline, respectively, instead of 2,2'-bipyridine.

[Er(tfac)$_3$(bipy)]: chemical formula: $C_{25}H_{20}ErF_9N_2O_6$. M_W: 782.68. Anal. Calcd. for $C_{25}H_{20}ErF_9N_2O_6$: C, 38.36; H, 2.58; Er, 21.37; F, 21.85; N, 3.58; O, 12.27. Found: C, 38.01; H, 2.56; N, 3.48.

[Er(tfac)$_3$(bath)]: chemical formula: $C_{39}H_{28}ErF_9N_2O_6$. M_W: 958.89. Anal. Calcd. for $C_{39}H_{28}ErF_9N_2O_6$: C, 48.85; H, 2.94; Er, 17.44; F, 17.83; N, 2.92; O, 10.01. Found: C, 48.81; H, 2.96; N, 2.98.

[Er(tfac)$_3$(5NO$_2$phen)]: chemical formula: $C_{27}H_{19}ErF_9N_3O_8$. M_W: 851.70. Anal. Calcd. for $C_{27}H_{19}ErF_9N_3O_8$: C, 38.08; H, 2.25; Er, 19.64; F, 20.08; N, 4.93; O, 15.03. Found: C, 38.01; H, 2.29; N, 4.98.

Physical and optical measurements

C, H, N elemental analyses were made using a Perkin Elmer CHN 2400 apparatus.

The crystal structures were elucidated by X-ray diffraction analysis. Prior to structural characterization, powder diffractograms were obtained using an ENRAF-NONIUS FR590 powder diffractometer equipped with an INEL120 detector (Debye-Scherrer geometry). Crystals of the compounds described here were heavily intergrown. Care had to be taken to choose one crystal with a dominant fragment, for data collection, but the existence of other smaller fragments cannot be excluded. Diffraction data were collected at 293(2) K using graphite monochromated MoKα (λ=0.71073 Å) radiation. Absorption corrections were made using SADABS.[26] The structures were solved by direct methods using SHELXS-97[27] and refined anisotropically (non-H atoms) by full-matrix least-squares on F^2 using the SHELXL-97 program.[27] PLATON[9] was used to analyse the structure and figure plotting. Disorder was observed in all three compounds. In the bipy compound, due to heavy disorder seen in the anions, several restraints in distances and ADPs had to be used. Atomic coordinates, thermal parameters and bond lengths and angles have been deposited at the Cambridge Crystallographic Data Centre (CCDC). Any request to the CCDC for these materials should quote the full literature citation and the reference number CCDC 997690-997692.

Differential scanning calorimetry (DSC) data were obtained on a DSC TA instrument mod Q100 v.9.0 with a heating rate of 10°C/min under a N_2 atmosphere. Infrared spectra were recorded with a Thermo Nicolet 380 FT-IR spectrometer in KBr pellets. Raman spectra were recorded with a FT-Raman Bruker FRA106 by using a near-IR (Nd: YAG, 1064.1 nm) laser to excite the samples. ^{1}H-NMR spectra were registered from deuterated methanol solutions (CD_3OD) on a Varian Mercury AS400 spectrometer equipped with a 5 mm Varian 4NUC probe. A single pulse sequence was used with 400.13 MHz of proton frequency and 376.459 MHz of fluorine frequency. The experiments for proton were acquired with 16 scans and pulse delay of 1 second and the fluorine experiments were acquired with 1000 scans and 1.5 seconds of pulse delay.

Optical absorption spectra in the UV-Vis region were recorded in diluted methanol solutions with a Shimazdu UV-2450 UV-Vis spectrophotometer. Photoluminescence measurements were conducted both in powder form and in 0.015 M deuterated methanol (CD_3OD) solutions. Visible photoluminescence spectra were excited with a 405 nm laser diode, and collected with a 0.303 focal length Shamrock spectrometer with an Andor Newton cooled CCD camera. Ligand lifetimes have been measured using an Edinburgh Instruments LifeSpec II fluorescence spectrometer, exciting the complexes at λ=405 nm with an Edinburgh Instruments EPL-405 picosecond pulsed diode laser (temporal pulse width at half-maximum about 80 ps), and using Edinburg Instruments F900 acquisition software. NIR photoluminescence spectra were measured by exciting the samples in powder form at the ligand absorption at around λ_{exc}=337 nm with a N_2 laser, and at λ_{exc}=532 nm resonantly with the $^4I_{15/2}\rightarrow{}^2H_{11/2}$ transition of the Er^{3+} absorption with a 500 mW cw laser diode, respectively. The emission was analyzed either with a Peltier-cooled InGaAs Hamamatsu pin photodiode G5851-21 at -25 ºC, for the samples in powder form, or with a N_2-cooled Ge detector, model PS-3 (Applied Detector Corp.), for the samples in solution, and a Horiba Jobin Yvon Triax 180 single-grating monochromator. For the excitation spectra, a Xenon arc lamp with a 1/8 m Oriel monochromator was used, detecting the emission at a fixed wavelength (1540 nm) using the Triax 180 monochromator. NIR photoluminescence time decay measurements for the samples in powder form were carried out by exciting the samples at 980 nm resonantly with the $^4I_{15/2}\rightarrow{}^4I_{11/2}$ transition of the Er^{3+} ions with an OPO at 10 Hz repetition rate (EKSPLA NT 342/3/UVE) and recorded using a Tektronix (model 3840) oscilloscope. For the samples in CD_3OD, indirect excitation of the ligands with a N_2 laser was used instead. Optical absorption and photoluminescence spectra have been measured at room temperature and all the emission spectra have been corrected by the spectral response of the experimental setup.

Device fabrication and evaluation

The structure of the devices is glass/ITO/PEDOT:PSS/[Er(tfac)$_3$(N,N-donor)]/Ca/Al. Pre-patterned ITO (140 nm) glass plates with four circular diodes (1 mm and 1.5 mm radii) were extensively cleaned, using chemical and UV–ozone methods, just before the deposition of the organic layers. The layer thicknesses were measured using an Alpha step 200 profilometer (Tenkor Instruments). PEDOT:PSS (CLEVIOS P VP AI 4083), previously filtered through a 0.45 µm hydrophobic filter, was deposited at 1500 rpm by spin-coating and then cured on a hot plate at 140ºC for 30 min. This process was repeated in order to obtain a 100 nm thickness layer, chosen to minimize failures associated to short circuit due to border effects. The active layers were then deposited from 5% methanol solutions by spin coating (1500 rpm) without further filtering and cured on a hot plate at 65ºC for 30 min in order to slowly and completely remove the solvent. The resulting thicknesses were 70 nm, 70 nm and 75 nm for [Er(tfac)$_3$(bipy)], [Er(tfac)$_3$(bath)] and [Er(tfac)$_3$(5NO$_2$phen)], respectively. The cathode (Ca/Al) was thermally evaporated in an atmosphere of 8×10^{-6} Torr on top of the organic layer surface and the structure was finally encapsulated using a glass cover attached by a bead of epoxy adhesive [EPO-TEK(730)]. All aforementioned processes were carried out in an inert atmosphere glovebox (<0.1 ppm O_2 and H_2O).

Current density-voltage (*J-V*) characteristics were measured using a semiconductor parameter analyser Agilent 4155C and a SMU pulse generator Agilent 41501B. A pulse train was used as input signal with a duty cycle of 0.2%. The refresh time between two consecutive pulses ensures long time operation without significant device degradation. Moreover, the *J–V* curve stability was achieved by gradually increasing the pulse amplitude up to the point where reproducible measurements were observed.

Electroluminescence spectra from the NIR-OLEDs were analyzed using a Spex (model 340E, f=34 cm) monochromator and detected with a N_2 cooled InAs Hamamatsu detector connected to a Stanford Research system SR530 locking amplifier, using 50% duty cycle wave form from a TTi40 MHz arbitrary waveform generator and a TREK-601C amplifier.

Acknowledgements

The authors would like to thank Prof. Carlos Zaldo for granting access to the ICMM-CSIC facilities, Dr. C. Force from NMR General Service at URJC, Prof. F. Lahoz (ULL) and Prof. P. Chamorro-Posada (UVa) for their insightful comments. P. Martín-Ramos thanks Iberdrola Foundation for its financial support. Support by MICINN (MAT2010-21270-C04-02, MAT2013-46649-C4-4-P, the Consolider-Ingenio 2010 Program MALTA CSD2007-00045 and the Spanish National Program of Infrastructure) and by EU-FEDER funds is gratefully acknowledged by La Laguna group. CEMDRX group is grateful to Fundaçao para a Ciencia e a Tecnologia (FCT) for providing funds under grant PTDC/FIS/102284/2008 and PEst-C/FIS/UI0036/2011. P. S. Pereira Silva acknowledges the scholarship SFRH/BPD/84173/2012 from FCT. Support by Comunidad Autónoma de Madrid under project S2009/MAT-1756 and by the Spanish Ministerio de Economía y Competitividad under projects MAT2009-08786, TEC2009-13991-C02-03 is acknowledged by URJC group.

Notes and references

[a] Advanced Materials Laboratory, ETSIIAA, Universidad de Valladolid, Avenida de Madrid 44, 34004, Palencia, Spain. E-mail: mgil@iaf.uva.es; Tel: +34 979 108347.
[b] Escuela Superior de Ciencias Experimentales y Tecnología (ESCET). Universidad Rey Juan Carlos. C/ Tulipán s/n, Móstoles, 28933 Madrid, Spain. E-mail: carmen.coya@urjc.es; Tel:
[c] Department of Physics and MALTA Consolider Team, Universidad de La Laguna, E-38200 San Cristóbal de La Laguna, Santa Cruz de Tenerife, Spain. E-mail: vlavin@ull.edu.es; Tel: +34 922 318321.
[d] CEMDRX, Physics Department, Universidade de Coimbra, Rua Larga, P-3004-516 Coimbra, Portugal. E-mail: manuela@pollux.fis.uc.pt; Tel: +351 239 410648

† Electronic Supplementary Information (ESI) available: PL emission in the NIR range in CD_3OD diluted solutions upon ligand excitation in the UV. CCDC reference numbers 997690-997692. See DOI: 10.1039/b000000x/

‡ This wavelength has been chosen for consistency reasons, provided that for the measurements of the ligand emission-associated PL decay time in the visible region a picosecond laser at 405 nm needs to be used so as to improve precision (the guaranteed pulse width for an EPL-405 is <100 ps, ten times shorter than those guaranteed for the pulsed LED available at 280 nm).

1. S. I. Weissman, *J. Chem. Phys.*, 1942, **10**, 214.
2. Y. Kawamura, Y. Wada, M. Iwamuro, T. Kitamura and S. Yanagida, *Chem. Lett.*, 2000, DOI: 10.1246/cl.2000.280, 280; R. J. Mears and S. R. Baker, *Opt. Quant. Electron.*, 1992, **24**, 517.
3. Y. Zheng, J. Lin, Y. Liang, Q. Lin, Y. Yu, Q. Meng, Y. Zhou, S. Wang, H. Wang and H. Zhang, *J. Mater. Chem.*, 2001, **11**, 2615; Y. Hasegawa, Y. Kimura, K. Murakoshi, Y. Wada, J.-H. Kim, N. Nakashima, T. Yamanaka and S. Yanagida, *J. Phys. Chem.*, 1996, **100**, 10201; J. Yuan and K. Matsumoto, *Anal. Sci.*, 1996, **12**, 31; G. Mancino, A. J. Ferguson, A. Beeby, N. J. Long and T. S. Jones, *J. Am. Chem. Soc.*, 2005, **127**, 524; G. E. Buono-core, H. Li and B. Marciniak, *Coord. Chem. Rev.*, 1990, **99**, 55; J. H. Melman, T. J. Emge and J. G. Brennan, *Inorg. Chem.*, 2001, **40**, 1078; L. D. Carlos, C. De Mello DonegÁ, R. Q. Albuquerque, S. Alves, J. F. S. Menezes and O. L. Malta, *Mol. Phys.*, 2003, **101**, 1037.
4. P. Martín-Ramos, C. Coya, Á. L. Álvarez, M. Ramos Silva, C. Zaldo, J. A. Paixão, P. Chamorro-Posada and J. Martín-Gil, *J. Phys. Chem. C*, 2013, **117**, 10020.
5. P. Martín-Ramos, M. R. Silva, C. Coya, C. Zaldo, Á. L. Álvarez, S. Álvarez-García, A. M. Matos Beja and J. Martín-Gil, *J. Mater. Chem. C*, 2013, **1**, 2725.
6. P. Martín-Ramos, P. S. Pereira da Silva, V. Lavín, I. R. Martín, F. Lahoz, P. Chamorro-Posada, M. Ramos Silva and J. Martín-Gil, *Dalton Trans.*, 2013, **42**, 13516.
7. G. Santos, F. J. Fonseca, A. M. Andrade, V. Deichmann, L. Akcelrud, S. S. Braga, A. C. Coelho, I. S. Gonçalves, M. Peres, W. Simões, T. Monteiro and L. Pereira, *J. Non-Cryst. Solids*, 2008, **354**, 2897.
8. A. G. Orpen, L. Brammer, F. H. Allen, O. Kennard, D. G. Watson and R. Taylor, *Dalton Trans.*, 1989, DOI: 10.1039/dt98900000s1, S1.
9. A. L. Spek, *J. Appl. Crystallogr.*, 2003, **36**, 7.
10. C. R. S. Morais, C. G. Gameiro, P. A. Santa-Cruz, S. Alves Jr, L. E. B. Soledade and A. G. Souza, *J. Therm. Anal. Calorim.*, 2007, **87**, 887.
11. F. Marandi, R. Rutvand, M. Rafiee, J. H. Goh and H.-K. Fun, *Inorg. Chim. Acta*, 2010, **363**, 4000.
12. Y. Hasegawa, S.-i. Tsuruoka, T. Yoshida, H. Kawai and T. Kawai, *J. Phys. Chem. A*, 2008, **112**, 803.
13. L.-J. Bian, H.-A. Xi, X.-F. Qian, J. Yin, Z.-K. Zhu and Q.-H. Lu, *Mater. Res. Bull.*, 2002, **37**, 2293.
14. J. A. Fernandes, R. A. Sá Ferreira, M. Pillinger, L. D. Carlos, J. Jepsen, A. Hazell, P. Ribeiro-Claro and I. S. Gonçalves, *J. Lumin.*, 2005, **113**, 50; José A. Fernandes, Rute A. S. Ferreira, M. Pillinger, Luís D. Carlos, Isabel S. Gonçalves and Paulo J. A. Ribeiro-Claro, *Eur. J. Inorg. Chem.*, 2004, **2004**, 3913.
15. J. Guo, L. Fu, H. Li, Y. Zheng, Q. Meng, S. Wang, F. Liu, J. Wang and H. Zhang, *Mater. Lett.*, 2003, **57**, 3899.
16. C. Görller-Walrand and K. Binnemans, in *Handbook on the physics and chemistry of rare earths*, eds. K. A. Gschneidner and L. Eyring Elsevier BV, Amsterdam, 1998, vol. 25, ch. 167, pp. 101.
17. S. A. Davis and F. S. Richardson, *Inorg. Chem.*, 1984, **23**, 184.
18. M. Irfanullah and K. Iftikhar, *J. Fluoresc.*, 2010, **21**, 81.

19. D. B. A. Raj, S. Biju and M. L. P. Reddy, *Inorg. Chem.*, 2008, **47**, 8091; C. Xu, *Monatsh. Chem.*, 2010, **141**, 631.
20. B. Kokuoz, J. R. DiMaio, C. J. Kucera, D. D. Evanoff and J. Ballato, *J. Am. Chem. Soc.*, 2008, **130**, 12222.
21. Z. Li, J. Yu, L. Zhou, H. Zhang, R. Deng and Z. Guo, *Org. Electron.*, 2008, **9**, 487; X. Li, Z. Si, C. Pan, L. Zhou, Z. Li, X. Li, J. Tang and H. Zhang, *Inorg. Chem. Commun.*, 2009, **12**, 675; P. Martín-Ramos, M. D. Miranda, M. R. Silva, M. E. S. Eusebio, V. Lavín and J. Martín-Gil, *Polyhedron*, 2013, **65**, 187; M. Ramos Silva, P. Martín-Ramos, J. T. Coutinho, L. C. J. Pereira and J. Martín-Gil, *Dalton Trans.*, 2014, **43**, 6752.
22. Y. Lv, J. Zhang, L. Wang, W. Cao and Z. Xu, *J. Lumin.*, 2008, **128**, 117; V. A. F. Deichmann, J. B. M. Novo, A. Cirpan, F. E. Karasz and L. Akcelrud, *J. Braz. Chem. Soc.*, 2007, **18**, 330.
23. S. Naka, H. Okada, H. Onnagawa and T. Tsutsui, *Appl. Phys. Lett.*, 2000, **76**, 197.
24. F. Wei, Y. Z. Li, G. Z. Ran and G. G. Qin, *Opt. Express*, 2010, **18**, 13542.
25. R. J. Curry, W. P. Gillin, A. P. Knights and R. Gwilliam, *Appl. Phys. Lett.*, 2000, **77**, 2271.
26. G. Sheldrick, University of Göttingen, Göttingen, Germany, 1996.
27. G. M. Sheldrick, *Acta Crystallogr. Sect. A: Found. Crystallogr.*, 2007, **64**, 112.